Physics of Plasmas

RESEARCH ARTICLE | MAY 14 2024

Study of impurity behavior in JET-ILW hybrid scenario with deuterium, tritium, and deuterium–tritium plasmas

Special Collection: Proceedings of PLASMA 2023 - International Conference on Research and Applications of Plasmas

N. Wendler ; A. Chomiczewska ; W. Gromelski ; E. Kowalska-Strzęciwilk; I. Ivanova-Stanik ; C. D. Challis; J. Hobirk ; A. Kappatou ; E. Lerche; P. Carvalho ; I. Coffey ; G. Pucella ; E. Giovannozzi ; JET Contributors,; Eurofusion Tokamak Exploitation Team

Phys. Plasmas 31, 052506 (2024)
https://doi.org/10.1063/5.0207200

Physics of Plasmas ARTICLE pubs.aip.org/aip/pop

Study of impurity behavior in JET-ILW hybrid scenario with deuterium, tritium, and deuterium–tritium plasmas

Cite as: Phys. Plasmas **31**, 052506 (2024); doi: 10.1063/5.0207200
Submitted: 6 March 2024 · Accepted: 25 April 2024 ·
Published Online: 14 May 2024

N. Wendler,[1,a)] A. Chomiczewska,[1] W. Gromelski,[1] E. Kowalska-Strzęciwilk,[1] I. Ivanova-Stanik,[1] C. D. Challis,[2] J. Hobirk,[3] A. Kappatou,[3] E. Lerche,[4] P. Carvalho,[2] I. Coffey,[2] G. Pucella,[5] E. Giovannozzi,[5] JET Contributors,[b)] and Eurofusion Tokamak Exploitation Team[c)]

AFFILIATIONS

[1]Institute of Plasma Physics and Laser Microfusion, Warsaw, Poland
[2]United Kingdom Atomic Energy Authority, Culham Campus, Abingdon, Oxfordshire OX14 3DB, United Kingdom
[3]Max-Planck-Institut für Plasmaphysik, Garching, Germany
[4]LPP-ERM/KMS, Brussels, Belgium
[5]Fusion and Nuclear Safety Department, ENEA, Frascati, Italy

Note: This paper is part of the Special Topic, Proceedings of PLASMA 2023 - International Conference on Research and Applications of Plasmas.
[a)]**Author to whom correspondence should be addressed:** natalia.wendler@ifpilm.pl
[b)]See the author list of C. F. Maggi *et al.*, "Overview of T and D-T results in JET with ITER-like wall," in Nuclear Fusion special issue: Overview and summary papers from the 29th Fusion Energy Conference, London, UK, 16–21 October, 2023.
[c)]See the author list of E. Joffrin *et al.* "Progress on an exhaust solution for a reactor using EUROfusion multi-machines capabilities" in Nuclear Fusion Special Issue: Overview and Summary Papers from the 29th Fusion Energy Conference, London, UK, 16–21 October, 2023.

ABSTRACT

Experimental campaigns at the Joint European Torus with an ITER-like Be/W wall with pure deuterium (D), tritium (T), and deuterium–tritium (DT) were a unique opportunity to explore various aspects related to the ITER operation. One of the most important challenges in recent years was the development of the hybrid scenario for D-T, based on reference deuterium and tritium plasmas. This kind of scenario, one of the foreseen for ITER, is characterized by a low current plasma and a high normalized beta β_N factor compared to the parallel optimized baseline scenario [Hobirk *et al.,* Plasma Phys. Controlled Fusion **54**, 095001 (2012)]. As the experiments have shown, controlling the plasma edge in the different phases of the hybrid scenario becomes more difficult with higher isotope mass, and therefore, are also in risk of impurity accumulation [Hobirk *et al.*, Nucl. Fusion **63**, 112001 (2023)]. For this reason, investigation of the impurity behavior, as well as their control, constituted the crucial issue. The present contribution aims to compare mid-Z and high-Z impurities behavior within H-mode hybrid discharges in D and T plasmas, as well as D and DT plasmas. Detailed analysis shows that in the H-mode regime in the hybrid scenario, higher impurity radiation is observed for DT in comparison to D plasmas, as well as for T compared to D plasmas. Additionally, it was noticed that the most significant contribution to the plasma radiated power comes from W and to a lesser extent from Ni (∼10%). Moreover, it was found that an earlier transition from small edge localized modes (ELMs) to ELM-free phase can result in the earlier increase in impurities.

I. INTRODUCTION

In 2021, the second JET deuterium–tritium experimental campaign (DTE2) with a substantial tritium concentration (i.e., comparable with or greater than the deuterium concentration) was carried out in conditions relevant to ITER and future fusion power plants. This second JET D-T campaign, after the first one (DTE1), which took place in 1997, led to the record high fusion power and energy values in steady plasma conditions in tokamaks that has been achieved for

Tritium-rich hybrid plasma with D:T ratio 15:85 for pulse #99 971 ($I_p = 2.5$ MA, $B_T = 3.86$ T).[3] In this discharge, it was possible to produce a fusion power of about 11 MW averaged over 5 s. Moreover, during the recent JET DTE2 campaign, a hybrid scenario for the first time has been also run in DT with a ratio 50:50. The best stationary pulse in 50:50 DT plasmas, namely, #99 869, achieved 7.4 MW of fusion power (P_{fus}) over 5 s, with ~33 MW injected NBI and ICRH heating powers. The mentioned JET ILW Hybrid scenario,[1] along with the baseline scenario,[4] is one of the main regimes exploited during the recent experimental campaigns on JET-ILW in H-mode plasma type-I edge localized modes (ELMs). To obtain good confinement, this approach uses high poloidal beta (β_p) with moderate plasma current $I_p = 2.3$ MA, high toroidal magnetic field $B_T = 3.45$ T as well as relatively flat q profile ($q_0 \geq 1$) and low core collisionality (central ion temperature T_{i0} > central electron temperature $T_{e0} \geq 8$ keV).[2] Furthermore, this kind of plasma scenario relies on high auxiliary heating power, namely, ≤32 MW of NBI and ≤4 MW of ICRH.

To achieve the highest possible fusion efficiency, it was necessary to optimize the hybrid scenario on JET by its development initially in D, later in T and finally in DT plasmas.[2] Each stage of optimization involved addressing different challenges. In the case of pure D, it was necessary to solve, among other things, the heat load issues resulting from the 37 MW of power injected in the ITER-like Be/W environment, to keep radiation at the edge and in the core under control, also avoiding MHD instabilities and achieving high neutron rates.[2] Then, in the T hybrid plasmas, it was again highly important to keep the radiation controlled. On the other hand, DT hybrid plasmas were optimized mainly for radiation-stable H-mode entry phase, improved performance, and good impurity control due to the edge impurity screening (strong T_i gradients outside the pedestal region, which prevent impurity influx from SOL).[5] Furthermore, as part of the hybrid scenario optimization in D, T, and DT plasmas also a detailed optimization of the plasma phases, such as the current ramp-up (Ohmic) phase, the H-mode entry phase, as well as the steady H-mode phase, have been performed. What is also relevant, on the basis of the detailed analysis of fast bolometry signals, it was found that in the optimized hybrid pulses, two different regimes can be distinguished, as is described in Ref. 5. In the first regime, the high-Z impurities are controlled by ELM flushing and the inward transport of impurities between ELMs can be expected. In the second regime with peripheral impurity screening, an outward transport of impurities between ELMs and, therefore, screening can be observed.[5]

The main difficulty in achieving the possible highest performance pulse in the frame of the DTE2 campaign was uncontrolled core impurity accumulation.[3] Thereby, investigation of the impurity behavior, as well as their control during almost every phase of hybrid plasmas, was one of the most crucial issues. For this reason, in this paper, we concentrate on the analysis of impurity behavior in the JET hybrid pulses that were performed in D, DT (with a ratio 50:50) and T plasmas at 2.3 MA with a magnetic field strength of ≈3.4 T. As part of this study, we compared mid-Z [e.g., nickel (Ni), copper (Cu), iron (Fe)] and high-Z [tungsten (W)] impurities behavior within D, T, and DT plasmas. In addition, we also investigated how various impurities behave in particular, phases of the hybrid discharges, which were optimized.

The presented analyses are primarily based on data collected by the VUV survey spectrometer[6,7] (known as KT2 at JET) and bolometry diagnostic.[8] The lines of sight of the two aforementioned systems are shown in Fig. 1. Data from the first system are mainly used for quantitative measurement of mid-Z impurities based on the method described in Ref. 9. Moreover, using these data, it is also possible to determine the intensity of different W ionization stages (W^{14+} – W^{35+}) from quasicontinuum in VUV spectra,[10] named I_W. The method used to determine I_W assumes avoidance of potential interference from other lines in the spectrum, especially from copper (Cu). Importantly, due to the non-working XUV diagnostic (known as KT7/3 at JET), which was usually used for studies described in Refs. 11–13, quantitative analysis of W was impossible. In turn, the second mentioned diagnostic, among other things, can provide bolometry reconstructions and radiation profiles. However, it should be noted that many of the hybrid pulses presented in this work involved the use of the Tritium Introduction Modules (TIM)15, resulting in contaminated signals for the horizontal bolometer camera. Therefore, the contribution from TIM15 was removed by iteratively lowering the signal levels on the horizontal camera until the reconstruction provided an output that balanced well the data from both cameras.[14]

II. STATISTICAL IMPURITY ANALYSIS FOR THE HYBRID PULSES IN DEUTERIUM AND DEUTERIUM–TRITIUM PLASMAS

Presented in this section analysis of impurity behavior has been performed for the set of hybrid pulses with D:T ratio 50:50, obtained during experimental campaigns in D (C38C and C42) and DT (DTE2). In these pulses, NBI and H minority ICRF heating power were kept at comparable levels, while the plasma current and toroidal field were, respectively, Ip = 2.3 MA and $B_T = 3.4$ T. To compare plasma radiation and various impurities in D and DT, values of particular plasma parameters were averaged over t_{NBI}+1.5 s to t_{NBI}+2.0 s

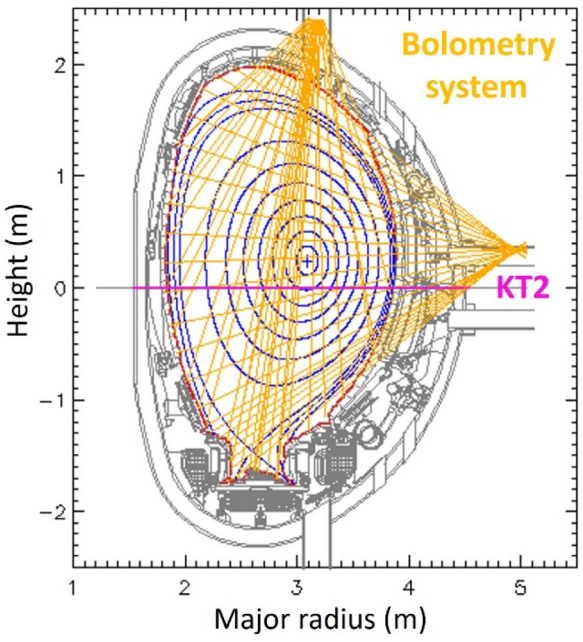

FIG. 1. The lines of sight of bolometry diagnostic (orange) as well as KT2 (magenta) VUV spectrometer with the magnetic equilibrium of JET pulse No: 99914 at 9 s.

(where t is the start of NBI heating). For the pulses analyzed in this section, several things are especially relevant. First, within the defined time range, a systematic trend for higher plasma confinement in DT compared to D was observed. Furthermore, pulses from the C42 experimental campaign appeared to have slightly worse confinement in comparison to C38C plasmas. A similar trend can be seen for the line integrated edge density, which achieves the highest values for DT plasma (Fig. 2), whereas the values of the edge ion temperature are comparable in all analyzed pulses.

What is also very important in the context of impurity analysis, although the pulses in the C42 experimental campaign have been performed as D engineering references, the C38 pulses had much later gas injection times, as well as lower gas injection rates (Fig. 3). In addition, it is worth noting that no correlation between change in the ELM frequency and the previously mentioned plasma parameters, such as $n_{e,edge}$ and $T_{i,edge}$, was found.

At the beginning of this study, the total radiated power (estimated from bolometer measurements) for different plasma mixtures was compared. As is shown in Fig. 4, the highest values of $P_{rad,total}$ were observed for DT plasmas. In turn, in the case of D pulses, slightly higher total radiation for data points at the same $P_{in} + P_{alpha}$ was found for C38C plasmas in comparison to C42 discharges. In this regard, it was important to find out which plasma impurities have a decisive influence on the observed plasma radiation.

For this reason, in the next step, radiation from mid-Z impurities (based on impurity density measurements from VUV diagnostic and the appropriate cooling rates), such as Ni, Cu, and Fe, as well as I_W were investigated. As can be seen from Fig. 5, I_W, which is measured closer to the pedestal region, was higher in DT pulses in comparison to D discharges. Moreover, the estimated I_W is well correlated with the total radiated power. On the other hand, from all the mid-Z impurities studied, Ni has the largest contribution to $P_{rad,total}$, but not exceeding ~10% (Fig. 5).

It is worth emphasizing that radiation from Ni occurs mainly for $T_e \approx 2$ keV, closer to the edge of the confined plasma region. In addition, it was also observed that radiation from Ni in D pulses was higher for C38C plasmas in comparison to C42 plasmas, which can be explained by different gas injection rates. As previously mentioned, pulses from the C38 experimental campaign had lower gas injection rates compared to C42 pulses. This, in consequence, could lead to increased Ni radiation. A similar trend of decreasing $P_{rad,Ni}$ with increasing gas injection rate was observed in other experiments with hybrid plasmas, which were a preparation for the JET D-T campaigns, as described in Ref. 12. Furthermore, since ELM frequency increases with the gas injection rates, in C38C plasmas lower ELM frequency compared to C42 plasmas was observed (Fig. 6), which may also result in higher Ni impurity radiation. In turn, radiation from other mid-Z impurities, such as Cu and Fe, contribute negligibly to the total radiation power and there are no clear differences in their behavior between D and DT plasmas. For this reason, they will not be discussed further.

Given that radiation from Ni constitutes about 10% of the $P_{rad,total}$ and the contribution from other mid-Z impurities is negligible,

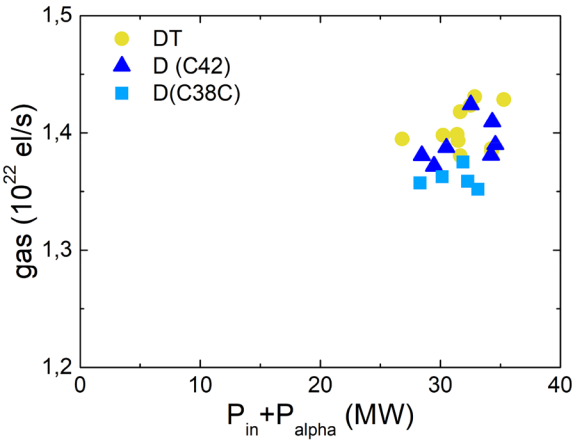

FIG. 3. The gas flow injection rate as a function of the sum of input and the alpha particles powers for DT and D plasmas.

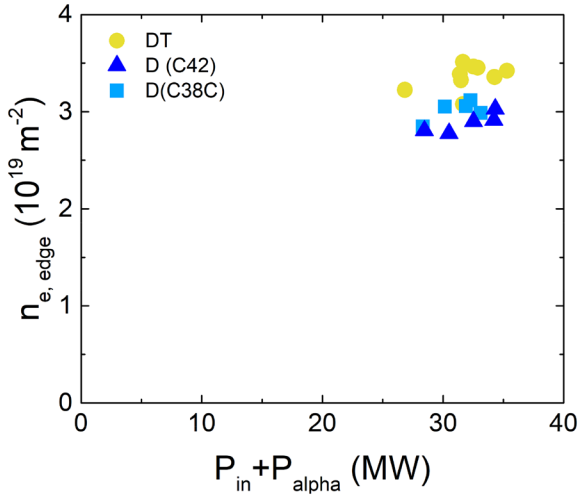

FIG. 2. The edge density as a function of the sum of input and the alpha particles powers for DT and D plasmas.

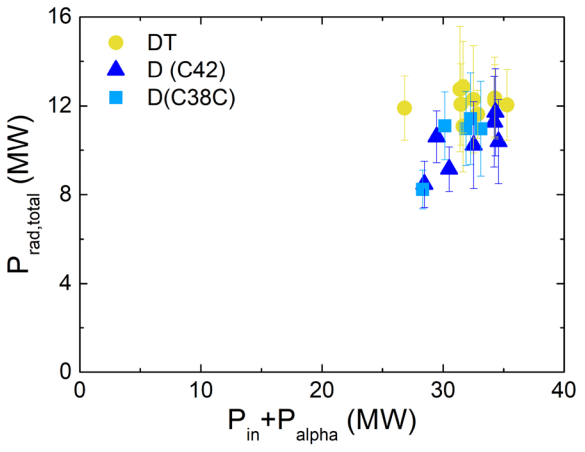

FIG. 4. The total radiated power as a function of the sum of input and the alpha particles powers for DT and D plasmas.

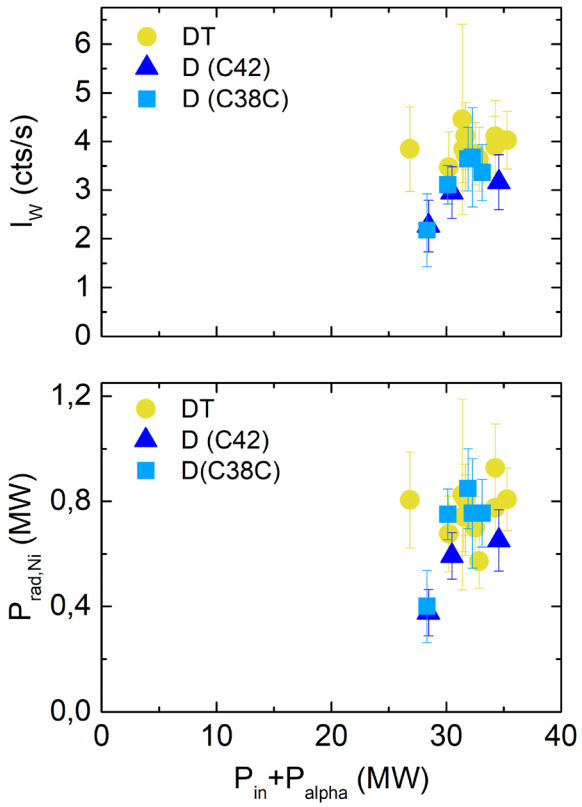

FIG. 5. The intensity of the W-ion ($W^{14+} - W^{35+}$) (on the top) and Nickel radiated power (on the bottom) as a function of the sum of input and the alpha particles power for DT and D plasmas.

it can be assumed that the rest of the radiation contributing to total radiated power comes mainly from high-Z impurities, namely, W. Therefore, it can be concluded that the contribution from W to the $P_{rad,total}$ was much more significant than from other mid-Z impurities in both investigated plasma mixtures—D and DT. In turn, the second significant impurity, in terms of radiated power, was Ni.

III. ENGINEERING MATCH WITH DEUTERIUM AND DEUTERIUM–TRITIUM PLASMAS

The following section presents impurity analysis in the frame of engineering match (heating power and gas match) with D (#100 822, #100 878) and DT (#99 914, #99 950) plasmas at 2.3 MA with a magnetic field strength of ≈3.4 T. In this study, D plasmas differ from DT references in slightly lower plasma density (up to 10%) and lower plasma stored energy (up to 15%). As can be also observed in Fig. 7, there is an earlier gas puff request for DT pulses to compensate for faster D response of the inlet valves compared with T. Furthermore, due to the lack of data from KT2 diagnostic for #100 822, analysis related to $P_{rad,Ni}$ and I_w for this pulse, could not be performed.

As previously mentioned in Sec. I, to achieve high-performance hybrid pulses, it was necessary to develop them in D and T, to finely translate them into DT mixtures. What was also equally important, optimization of the different phases of the hybrid pulses was needed.[2] For this reason, in this part of the work, we concentrate on impurity

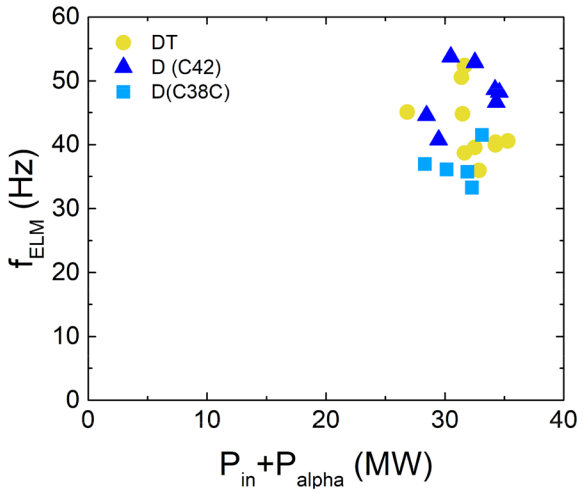

FIG. 6. ELMs frequency as a function of the sum of input and the alpha particles powers for DT and D plasmas.

behavior in two different phases of hybrid pulses in D and DT plasmas, which are as follows: H-mode access phase and H-mode (initial and steady) phase. Therefore, the main aim of this analysis is to investigate how the mass of the isotope affects the different phases of the pulses, especially in the context of plasma radiation and impurity behavior.

A. Engineering match with deuterium and deuterium-tritium plasmas—H-mode access phase

The greatest challenge during the optimization of the H-mode access phase (ELM free phase, occurring after the application of high external power), was the smooth transition from hot ion pedestal phase to Type I ELMy regime without impurity influx, neither strong pedestal density (n_{ped}) growth.[2] As it has been proven so far, H-mode access strongly depends on the plasma composition, indicating an isotope effect.[15,16] Thereby, it can be expected that inducing the first ELM in T and DT may be more difficult. Moreover, also different plasma-wall interactions that lead to higher Be/W sputtering, as well as different L-H thresholds, which will require adjusting the power should be assumed.[15,16] Additionally, the strong scaling of auxiliary heating power absorbed by the plasma with effective isotopic mass suggests that it may be easier to enter H-mode in T-rich plasmas in any DT fusion devices.[17] This, in turn, is a result of the increased absorption of RF power in T-rich plasmas in cases where RF is applied during the L-H transition phase. At the beginning of the analysis concerning the H-mode access phase, the transition from small ELMs to ELM-free H-mode in D and DT pulses was compared.

As shown in Fig. 8, DT references differ from D plasmas in a slightly earlier transition from small ELMs to ELM-free H-mode, resulting in a longer phase without ELMs. Moreover, this was accompanied by higher density increase at slightly lower edge ion temperature in DT plasmas (see Fig. 7). Therefore, as a consequence, the edge radiation which was estimated from channel 2 of the vertical bolometer camera (unaffected by TIM15) was higher in DT pulses during the ELM-free phase. In turn, in the case of D plasmas, $P_{rad,edge}$ was not only lower than in DT references but also very comparable in the two

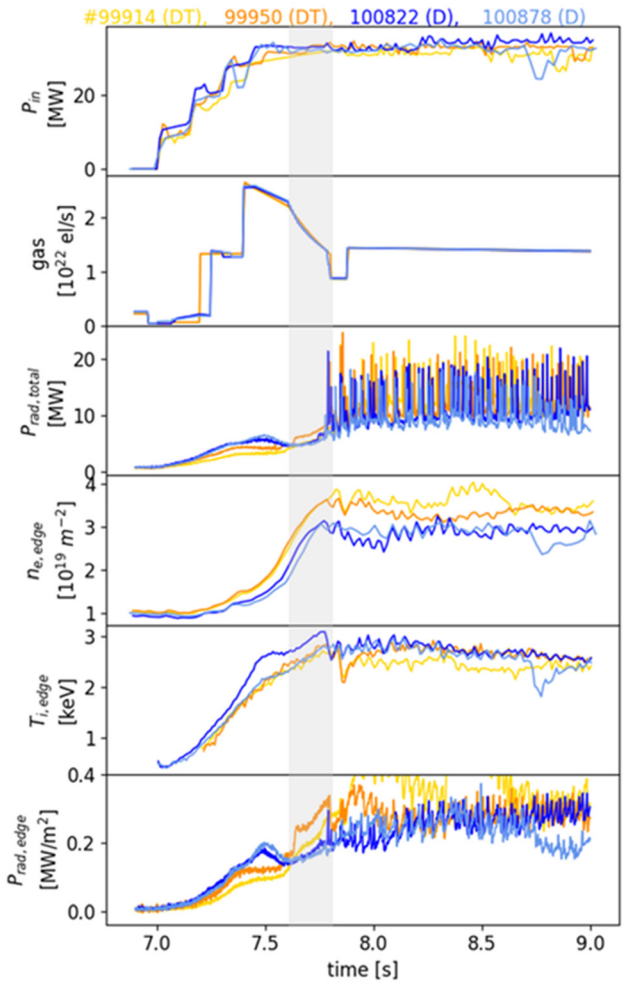

FIG. 7. Waveforms for D (#100 822 and #100 878) and DT (#99 914 and #99 950) pulses, showing from the top: heating power, the gas request rate, the total radiated power, the line integrated edge density, the edge ion temperature from CXRS at $R_{maj} = 3.72$ m. and the edge line averaged radiation from a vertical bolometer channel. The gray vertical bar denotes the ELM-free phase.

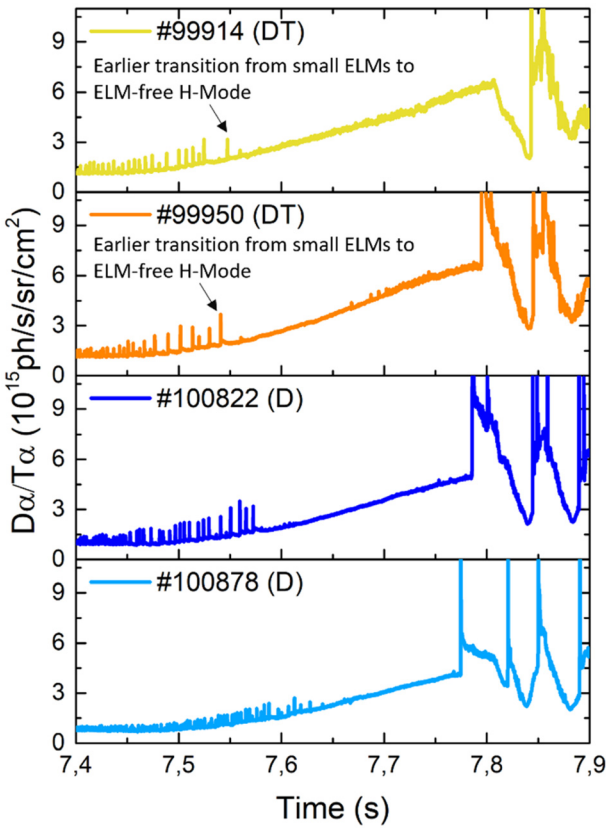

FIG. 8. Waveforms for D (#100 822 and #100 878) and DT (#99 914 and #99 950) pulses in the H-mode access phase showing D_α/T_α emission.

pulses studied, namely, #100 822 and #100 878. On the other hand, in the H-mode access phase (up to $t \approx 7.75$ s), I_W appears to be almost comparable in all investigated pulses, as illustrated in Fig. 9. In turn, as can be also seen, radiation from Ni takes similar values in both, D (#100 878) and DT (#99 950) plasmas. Moreover $P_{rad,Ni}$ remains almost constant for the entire H-mode access phase. However, what should be noted, the significant difference in Ni radiated power between two DT pulses—#99 914 and #99 950 was also observed.

In DT pulse #99 914, noticeably lower radiation from Ni compared to another DT plasmas #99 950 has been linked to the delayed start of ICRH heating (Fig. 10) since Ni impurities at JET are associated with the operation of ICRH antennas.[18] Moreover, this was further confirmed by the fact that at $t \approx 7.6$ s (time point associated with the ELM-free phase and the observed difference in $P_{rad,Ni}$), comparable electron density profiles for both DT pulses (#99 914 and #99 950) between $R_{maj} = 3.6$ and 3.8 m, where Ni was measured, are observed (Fig. 11). It was therefore possible to exclude the influence of density on the radiation from Ni.

Given the above, it can be concluded that in DT plasmas, slightly earlier transition from small ELMs to ELM-free H-mode as well as a longer phase may have led to the observed higher edge radiation in comparison to D plasmas.

B. Engineering match with deuterium and deuterium–tritium plasmas—Initial and steady ELMy H-mode phase

To establish high-performance pulse, it is necessary to achieve a steady H-mode phase (characterized by regular type I ELMs in high confinement mode) with high ion temperature and with no gradual increase in radiation at the same time. Therefore, the main aspects of a stationary high-performance hybrid discharge optimization, in particular, include sufficient high and reproducible NBI and ICRH power, as well as the appropriate amount of injected gas. As has been observed, larger input power is needed for high fusion performance. However, the mentioned performance is very sensitive to NBI power waveform. Another key factor that can ensure high performance is well-optimized gas flow. Excessive gas flow may lead to pedestal cooling and low performance. In this variant, also fast ELMs are observed,

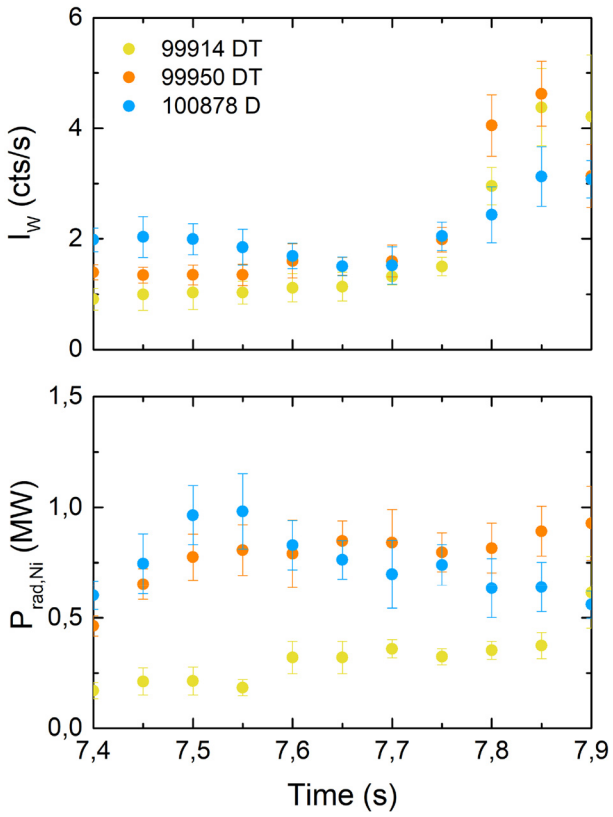

FIG. 9. Time traces of the intensity of the W-ion ($W^{14+} - W^{35+}$) (on the top) and nickel radiated power (on the bottom) for DT and D plasmas in the H-mode access phase.

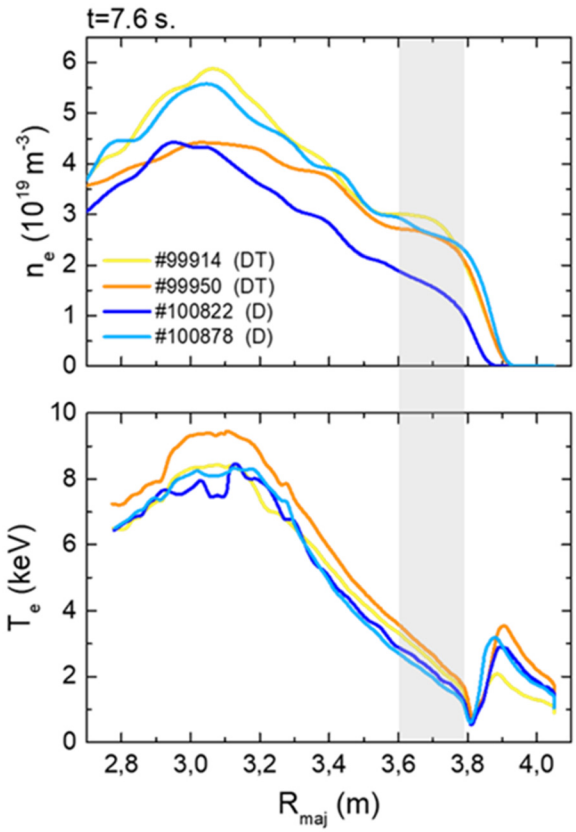

FIG. 11. The electron density (on the top) and the electron temperature (on the bottom) profiles for DT (#99 914 and #99 950) and D (#100 822 and #100 878) plasmas at t = 7.6 s during the H-mode access. The gray vertical bar denotes the range in which $P_{rad,Ni}$ was measured.

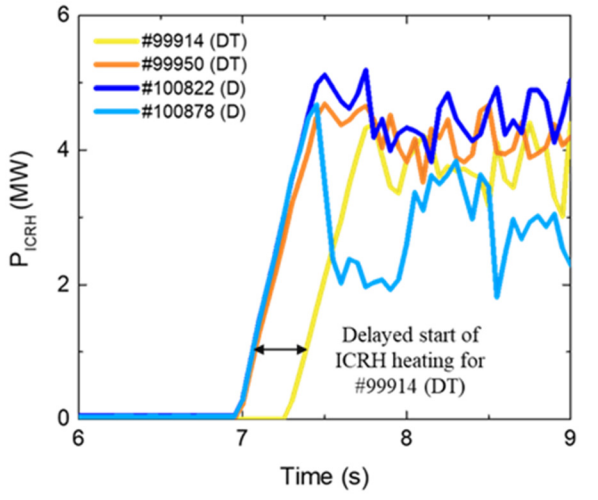

FIG. 10. Time traces of the ICRH power for D (#100 822 and #100 878) and DT (#99 914 and #99 950) pulses.

which are a positive aspect from the plasma impurity point of view. In turn, an insufficient amount of gas can also lead to significant decrease in plasma performance through the possible impurity influx or potential impurity accumulation. Moreover, ELMs besides gas injection rate, can be also controlled by other parameters, namely, plasma shape and strike position, as well as power through separatrix (P_{sep}), which is defined as the difference between input power (P_{in}) and bulk radiated power ($P_{rad,bulk}$). For plasma discharges in the hybrid scenario, as the P_{sep} increases, faster ELMs can be expected as well.[19] In contrast, for smaller P_{sep} values, slower ELMs and consequently potential accumulation of impurities can be observed.

Figure 12 shows how the ELMs in the analyzed pulses were changing during the ELMy H-mode phases. It can be seen that ELMs in DT and D plasmas differ in their amplitude—slightly larger ELMs in DT pulses in comparison to D [e.g., the average ELM amplitudes in the time range between 8.25 and 9.5 s are as follows: ~4.33 × 10^{15} ph/s/sr/cm^2 for #99 914 (DT), ~4.74 × 10^{15} ph/s/sr/cm^2 for #99 950 (DT), ~3.93 × 10^{15} ph/s/sr/cm^2 for #100 822 (D), and ~3.38 × 10^{15} ph/s/sr/cm^2 for #100 878 (D)]. Observed difference in ELMs had also an impact on plasma impurities. As has been proven so far, ELMs with higher frequency and lower amplitude in hybrid plasmas are

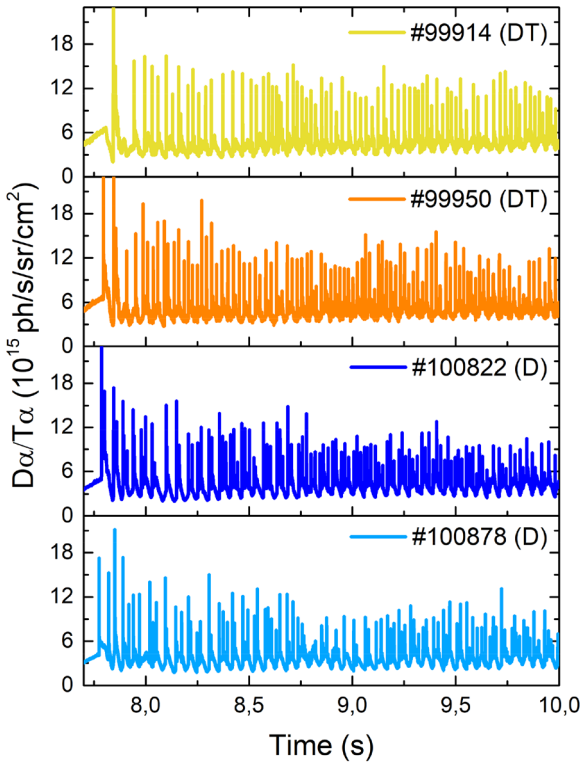

FIG. 12. Waveforms for D (#100 822 and #100 878) and DT (#99 914 and #99 950) pulses in the H-mode phase showing D_α/T_α emission.

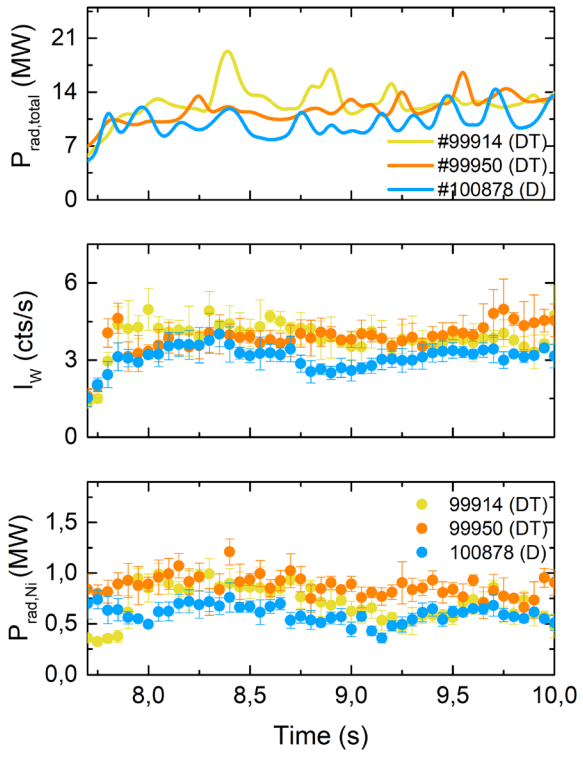

FIG. 13. Time traces of the $P_{rad,total}$ (on the top), intensity of the W-ion (W^{14+}–W^{35+}), and nickel radiated power (on the bottom) for DT and D plasmas in the H-mode phase.

responsible for the effective impurity flushing.[2,5] In practice, this means that, among other things, ELMs with lower amplitude flush out more W and, thus, leads to a reduction in the radiated power. Therefore, it can be stated that flushing action of the ELMs (especially in the context of W) is crucial for the control of radiation. As illustrated in Fig. 13, during the H-mode phase, $P_{rad,total}$, $P_{rad,Ni}$ as well as I_W values were noticeably higher for DT pulses. Moreover, in analyzed pulses, W and Ni were the largest contributors to the total radiated power; however, the contribution from Ni is much smaller in comparison to W and does not exceed 12% of $P_{rad,total}$. What is additionally important in terms of impurities control, both $P_{rad,Ni}$ and I_W values were almost stable during the entire H-mode phase in both investigated plasmas mixtures (D and DT). Thereby, no impurity accumulation was observed in any of the pulses under study. The provided observations on plasma impurities are also consistent with the fact that during the H-mode phase, in the case of DT plasmas, slightly higher edge density at the lower edge ion temperature was also visible (see Fig. 7) Moreover, not without significance is the fact that, as already shown in Sec. III A, DT plasmas exhibited slightly earlier transition from small ELMs to ELM-free H-mode, which also influenced increased plasma radiation in the H-mode phase.

IV. ENGINEERING MATCH WITH DEUTERIUM AND TRITIUM PLASMAS

As the analysis described in Sec. III shows, with the higher isotope mass (D vs DT), it may be more difficult to control plasma radiation in both phases—the H-mode access and the H-mode. Here, a comparison of the two pulses, one in D and the other in T, in terms of impurity behavior will be presented. The investigated pulses were characterized by the same engineering parameters and were performed at $B_T \approx 3.4$ T and $I_p \approx 2.3$ MA, with $P_{in} \approx 31$ MW. As can be seen from Fig. 14, the gas request waveforms for these two pulses are slightly different. This, in turn, is due to the reduced flow speed of T compared to D in the gas pipes.[2] For this reason, the gas request waveform for the D pulse has been adjusted in terms of slower T flow speed. Therefore, there was no delay in the arrival time of the gas in the presented pulses.

As in the previous analysis in Sec. III A, the study started with a comparison of the transition from small ELMs to ELM-free H-mode in D and T. As can be seen from Fig. 15, the ELM-free phase had started earlier in the T pulse, which was expected due to higher isotope mass. It can also be observed that in the T pulse there was an earlier edge density increase with an associated rapid increase in edge radiation (Fig. 14). In contrast to this case, in the D pulse, there was a significantly lower $P_{rad,edge}$ during the ELM-free phase. Moreover, in this plasmas also lower $n_{e,edge}$ at higher $T_{i,edge}$ (in comparison to T plasmas) was observed, which may indicate impurity screening. These observations are consistent with the results related to the $P_{rad,Ni}$ and I_W, as shown in Fig. 16. As can be seen, in T plasmas from $t \approx 7.4$ to $t \approx 7.8$ s (ELM-free phase), there is a gradual increase in $P_{rad,Ni}$ and I_w, which correlates with the increase in $P_{rad,edge}$. In turn, in D plasmas from $t \approx 7.6$ to $t \approx 7.8$ s (ELM-free phase), $P_{rad,Ni}$ behaves almost

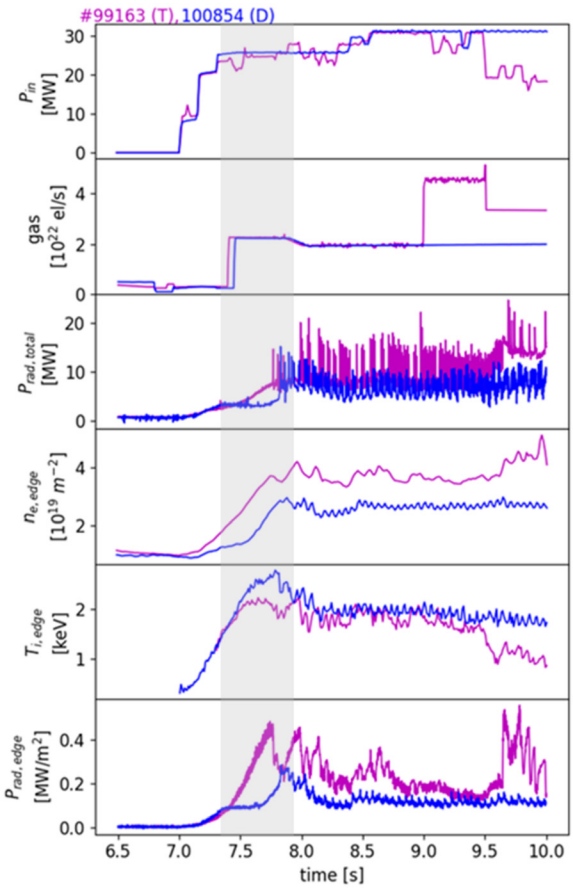

FIG. 14. Waveforms for D (#100 854) and T (#99 163) pulses, showing from the top: heating power, the gas request rate, the total radiated power, the line integrated edge density, the edge ion temperature from CXRS at $R_{maj} = 3.72$ m, and the edge line averaged radiation from a vertical bolometer channel. The gray vertical bar denotes the ELM-free phase.

stable, while in I_W there is some increase, but smaller than in T pulse. It is also worth noting that radiation from Ni during the H-mode access phase was higher for T plasmas.

As is presented in Fig. 17, in the steady H-mode phase of analyzed discharges, there is a noticeable difference in the amplitudes of the ELMs—larger ELMs in T pulses in comparison to the D pulse [e.g., the average ELM amplitudes in the time range between 8.5 and 9.25 s are $\sim 6.58 \times 10^{15}$ ph/s/sr/cm^2 for #99 163 (T) and $\sim 3.91 \times 10^{15}$ ph/s/sr/cm^2 for #100 854 (D) pulses]. Thus, also $P_{rad,total}$, $P_{rad,Ni}$, and I_W (Fig. 18) values are significantly higher in T plasmas. The increased radiation in the T pulse compared to D is not only correlated with the amplitude of the ELMs but may also be a consequence of an earlier transition from the small ELMs to ELM-free H-mode. On the other hand, in D pulse, $P_{rad,Ni}$, and I_W (both estimated closer to the plasma edge) take almost constant values throughout the H-mode phase which is linked to low and stable $P_{rad,edge}$, as well as ELMs amplitude. Additionally, it was found that in both pulses, the largest contribution to plasma radiation was from W as well as Ni, but to a much lesser extent. Furthermore, the results presented in this chapter confirm the

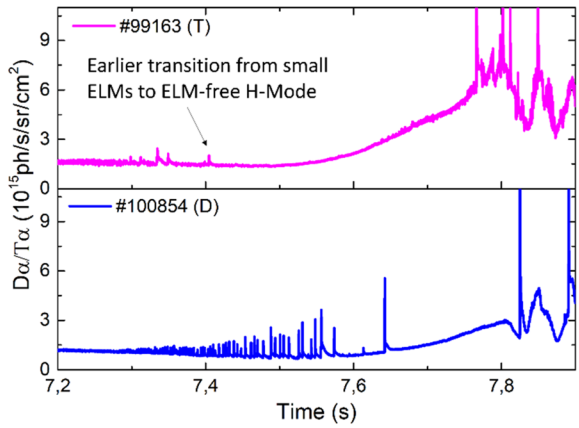

FIG. 15. Waveforms for D (#100 854) and T (#99 163) pulses in the H-mode access phase showing D_α/T_α emission.

observations from Sec. III that with the higher isotope mass, control of plasma radiation seems to be much more difficult. Moreover, it seems that the timing of the transition to ELM-free phase can determine the further evolution of the pulse.

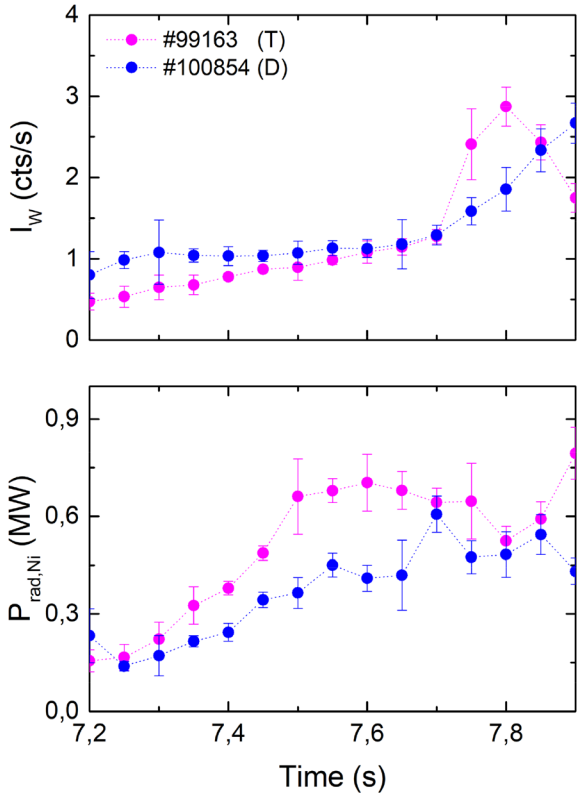

FIG. 16. Time traces of the intensity of the W-ion ($W^{14+} - W^{35+}$) (on the top) and nickel radiated power (on the bottom) for T and D plasmas in the H-mode access phase.

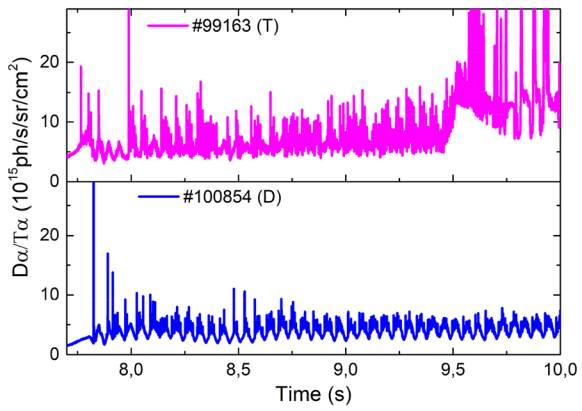

FIG. 17. Waveforms for D (#100 854) and T (#99 163) pulses in the H-mode phase showing D_α/T_α emission.

V. ACCESS TO H-MODE IN DEUTERIUM AND TRITIUM PLASMAS

As discussed before, one of the greatest challenges during the optimization of the H-mode access phase is impurity control, especially in DT and T plasmas. Since this issue is crucial in view of the operation of future thermonuclear devices using a plasma mixture that also contains T, in this section, another comparison of the D pulse with the T pulse is presented. This will provide an example of the possible undesirable effects due to the higher isotope mass (T) and, thus, the missing of ELM activity (for a longer time than in D plasmas) in the H-mode access phase. In the pulses here, in D (#97 977) and T (#99 272), which were performed at $I_p = 2.3$ MA and $B_T = 3.45$ T, the behavior of plasma impurities and radiation was investigated. As can be seen in Fig. 19, presented pulses are characterized by almost the same heating power and gas request waveforms.

Nevertheless, in the case of the T plasmas compared to the D pulse, several clear differences during the H-mode entry phase can be observed. First of all, in pulse #99 272, there is an earlier transition to the ELM-free phase and this phase is longer than in D plasmas (Fig. 20). Moreover, with the appearance of the first dithering ELMs in T pulse at about $t \approx 7.3$ s, the first clear differences in $n_{e,edge}$ between two pulses studied can be seen (higher $n_{e,edge}$ in T pulse compared to D). Therefore, the rapid and significant increase in edge radiation consequently leads to edge cooling, which is also consistent with a loss of impurity screening. As a result of this, increased radiation at the T

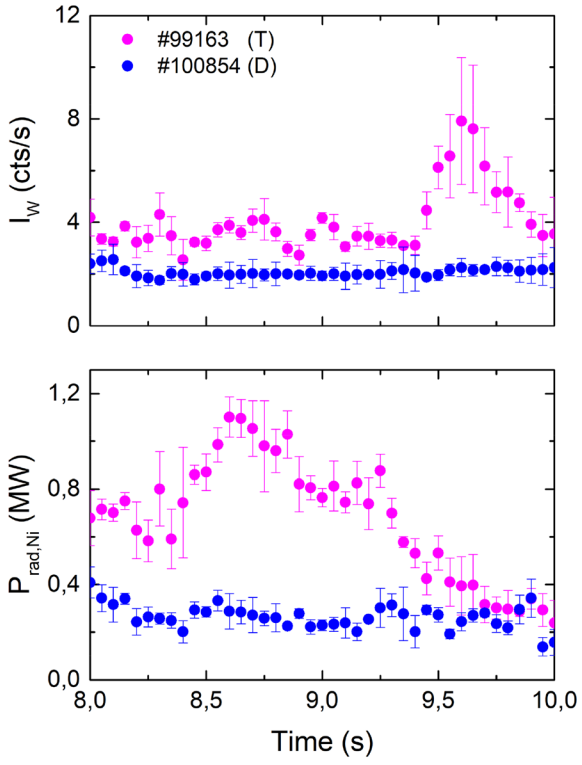

FIG. 18. Time traces of the intensity of the W-ion ($W^{14+} - W_{35+}$) (on the top) and nickel radiated power (on the bottom) for T and D plasmas in the H-mode phase.

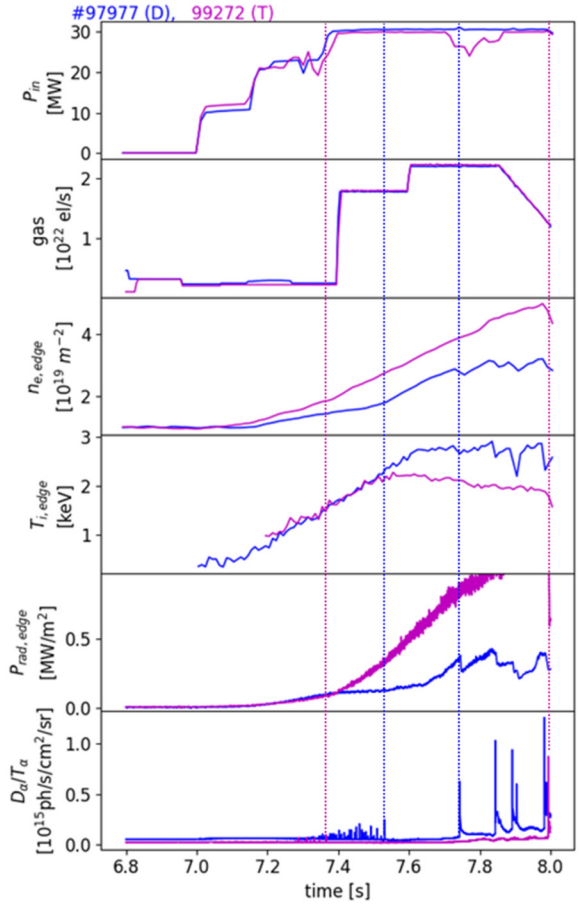

FIG. 19. Waveforms for D (#97 977) and T (#99 272) pulses, showing from the top: heating power, the gas request rate, the line integrated edge density, the edge ion temperature from CXRS at $R_{maj} = 3.72$ m, the edge line averaged radiation from a vertical bolometer channel and D_α/T_α emission. The magenta and blue vertical lines denote ELM-free phase in T and D pulse, respectively.

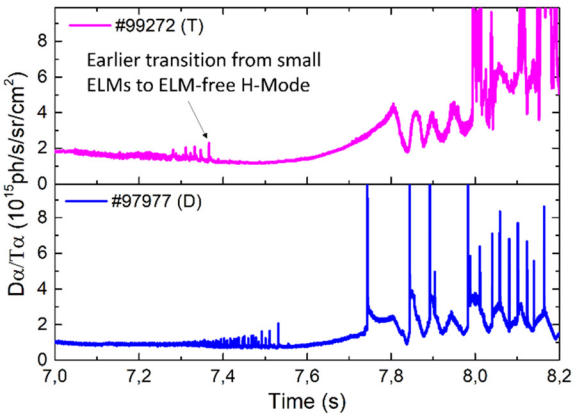

FIG. 20. Waveforms for D (#97 977) and T (#99 272) pulses in the H-mode access phase showing D_α/T_α emission.

plasma edge in comparison to the D pulse was observed, which is presented in Fig. 21.

Namely, it can be seen that from $t \approx 7.3$ s, which corresponds to the start of transition from small ELMs to ELM-free H-mode phase, in T pulse, there is a noticeable increase in radiation from Ni, which is also in line with the increase in $P_{rad,edge}$. Then, from $t \approx 7.9$ s, a greater increase in W intensity can be seen, which is also consistent with the $P_{rad,edge}$, while the Ni radiation appears to remain almost constant at the same time. The observed rapid increase in I_w, just before the H-mode phase, which starts in T pulse about $t = 7.8$ s is associated with a buildup of the density gradient at almost consant and low $T_{i,edge}$ (no T_i gradient screening). In such conditions, tungsten inward transport occurs, leading to the large W influx.[5] In turn, in the case of the D pulse, it was possible to avoid impurity influxes through the plasma edge because $T_{i,edge}$ increased before the significant $n_{e,edge}$ increases (see Fig. 19). Thus, effective impurity screening was established. This effect is also visible in Fig. 21, where $P_{rad,Ni}$, I_W, and $P_{rad,edge}$ are significantly lower than in T plasmas, and their values remain almost stable throughout the H-mode access phase. These observations are also confirmed by tomographic reconstructions performed for $t \approx 7.7$ s, which show that the radiated power density is mainly emitted from the LFS of the plasma and was at least several times higher for T pulse compared to D discharge (Fig. 22). Also, the radiation profiles, presented in Fig. 23, for $t \approx 7.7$ s, indicate that the radiation at the plasma edge was significantly higher for T in comparison to D plasma. It should be emphasized at this point that, despite the constraint mentioned in Sec. I, related to the interference of the tomographic reconstruction by TIM15 operation (concerning mainly the horizontal bolometer array), the presented accumulation on the LFS (Fig. 22) was provided by the vertical camera, which was unaffected by TIM15.

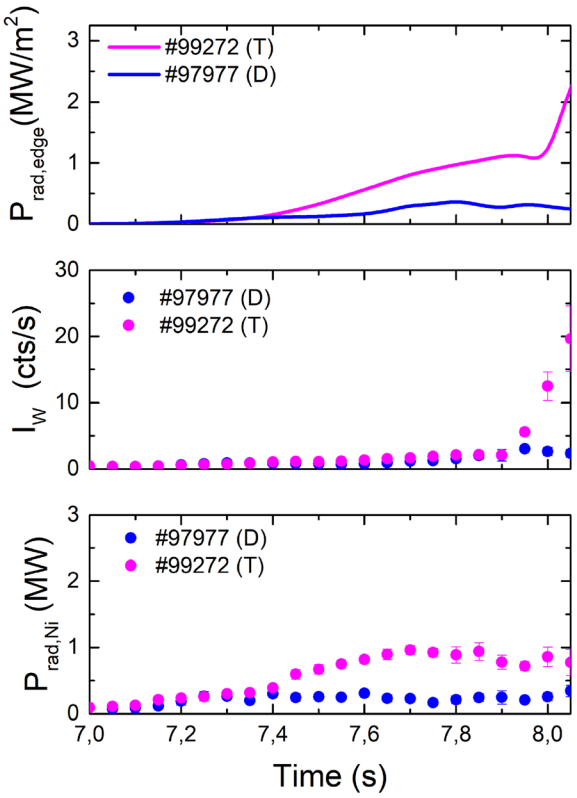

FIG. 21. Time traces of the $P_{rad,edge}$ (on the top), intensity of the W-ion ($W^{14+} - W^{35+}$), and nickel radiated power (on the bottom) for D and T plasmas in the H-mode access phase.

VI. CONCLUSIONS

During the recent DT campaign (DTE2) in JET-ILW tokamak with Be/W wall, high-performance hybrid discharges were carried out, in which record values of fusion power and energy in steady plasma conditions were achieved. The highest performance that has been obtained under the hybrid scenario could only be held for a few seconds, mainly because of gradual impurity accumulation. For this reason, the study of plasma impurities, and no less importantly, their control during the experiments performed has become one of the most crucial tasks. The results provided by this paper indicate that with higher isotope mass, controlling plasma radiation becomes more challenging. This is especially noticeable in the H-mode access phase, where an earlier transition from small ELMs to ELM-free H-mode in

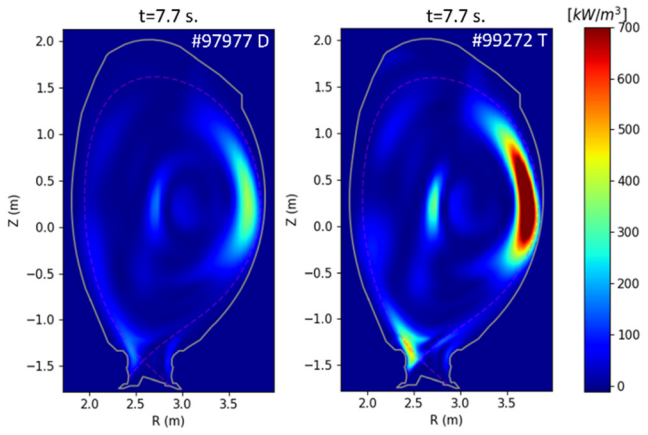

FIG. 22. Bolometry reconstructions for D (#97 977) and T (#99 272) pulses at $t = 7.7$ s from the H-mode access phase.

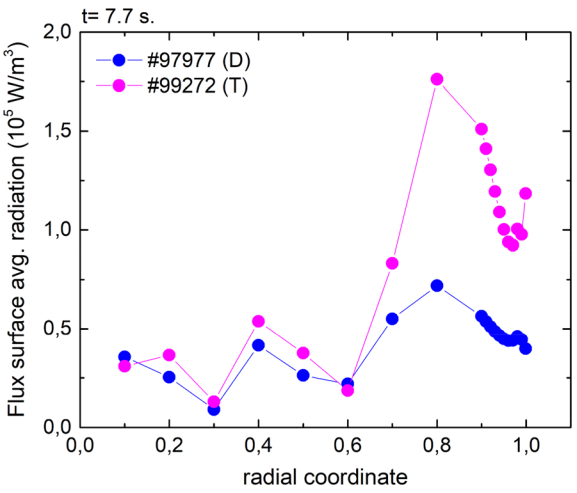

FIG. 23. The flux surface averaged profiles of the radiated density as a function of the normalized radius for D (#97 977) and T (#999 272) pulses at t = 7.7 s from the H-mode access phase.

DT and T plasmas, can result, for example, in increased radiation at the plasma edge due to a loss of impurity screening. Then, W and Ni are the largest contributors to plasma radiation. The situation was different for D pulses, where mainly effective impurity screening was observed. Its effects can be seen, among other things, in lower $P_{rad,edge}$ and, thus, also lower I_W and $P_{rad,Ni}$. Similarly, in the H-mode phase, higher $P_{rad,total}$, $P_{rad,Ni}$, and I_W were observed for plasmas mixtures with higher isotope mass, namely, in DT pulses in comparison to D, as well as in T compared to D pulses. Moreover, it was then found that the largest contribution to the total radiated power came from W and to a lesser extent from Ni. In addition, the results presented in this paper show that an earlier transition from small ELMs to ELM-free H-mode phase may result in an earlier increase in the amount of impurities. Furthermore, greater I_W, $P_{rad,Ni}$, and, in general, $P_{rad,total}$ during the H-mode phase in DT and T plasmas were also well correlated with the larger amplitude of ELMs.

ACKNOWLEDGMENTS

This scientific paper has been published as part of the international project co-financed by the Polish Ministry of Science and Higher Education within the programme called "PMW" for 2021–2024. This work has been carried out within the framework of the EUROfusion Consortium, funded by the European Union via the Euratom Research and Training Programme (Grant Agreement No 101052200—EUROfusion) and from the EPSRC (Grant No. EP/W006839/1). Views and opinions expressed are, however, those of the author(s) only and do not necessarily reflect those of the European Union or the European Commission. Neither the European Union nor the European Commission can be held responsible for them.

AUTHOR DECLARATIONS

Conflict of Interest

The authors have no conflicts to disclose.

Author Contributions

N. Wendler: Conceptualization (lead); Investigation (lead); Visualization (lead); Writing – original draft (lead). **A. Chomiczewska:** Investigation (supporting); Methodology (supporting); Software (equal); Writing – review & editing (supporting). **W. Gromelski:** Software (supporting); Writing – review & editing (supporting). **E. Kowalska-Strzeciwilk:** Investigation (supporting). **I. Ivanova-Stanik:** Investigation (supporting). **C. D. Challis:** Investigation (supporting); Writing – review & editing (supporting). **J. Hobirk:** Investigation (supporting); Writing – review & editing (supporting). **A. Kappatou:** Investigation (supporting); Writing – review & editing (supporting). **E. Lerche:** Investigation (supporting). **P. Carvalho:** Investigation (supporting); Resources (supporting); Writing – review & editing (supporting). **I. Coffey:** Resources (supporting). **G. Pucella:** Investigation (supporting). **E. Giovannozzi:** Investigation (supporting).

DATA AVAILABILITY

The data that support the findings of this study are available from the corresponding author upon reasonable request.

REFERENCES

[1]J. Hobirk, F. Imbeaux, F. Crisanti, P. Buratti, C. D. Challis, E. Joffrin, B. Alper, Y. Andrew, P. Beaumont, M. Beurskens *et al.*, "Improved confinement in JET hybrid discharges," Plasma Phys. Controlled Fusion **54**, 095001 (2012).
[2]J. Hobirk, C. D. Challis, A. Kappatou, E. Lerche, D. Keeling, D. King, S. Aleiferis, E. Alessi, C. Angioni, F. Auriemma *et al.*, "The JET hybrid scenario in deuterium, tritium and deuterium-tritium," Nucl. Fusion **63**, 112001 (2023).
[3]M. Maslov, E. Lerche, F. Auriemma, E. Belli, C. Bourdelle, C. D. Challis, A. Chomiczewska, A. Dal Molin, J. Eriksson, J. Garcia *et al.*, Nucl. Fusion **63**, 112002 (2023).
[4]L. Garzotti, D. Frigione, P. Lomas, F. Rimini, D. Van Eester, S. Aleiferis, E. Alessi, I. S. Carvalho, P. Carvalho, A. Chomiczewska *et al.*, "Development of high-current baseline scenario for deuterium-tritium high fusion performance at JET," in IAEA Fusion Energy Conference, 2023.
[5]A. R. Field, F. J. Casson, D. Fajardo, C. Angioni, C. D. Challis, J. Hobirk, A. Kappatou, H.-T. Kim, E. Lerche, A. Loarte *et al.*, Nucl. Fusion **63**, 016028 (2023).
[6]I. H. Coffey and R. Barnsley, Rev. Sci. Instrum. **75**, 3737 (2004).
[7]K. D. Lawson, I. H. Coffey, J. Zacks, M. F. Stamp, and JET-EFDA Contributors. "An absolute sensitivity calibration of the JET VUV SPRED spectrometer," J. Instrum. **4**, P04013 (2009).
[8]A. Huber, K. McCormick, P. Andrew, P. Beaumont, S. Dalley, J. Fink, J. C. Fuchs, K. Fullard, W. Fundamenski, L. C. Ingesson *et al.*, "Upgraded bolometer system on JET for improved radiation measurements," Fusion Eng. Des. **82**, 1327–1334 (2007).
[9]A. Czarnecka, K.-D. Zastrow, J. Rzadkiewicz, I. H. Coffey, K. D. Lawson, M. G. O'Mullane, JET-EFDA Contributors *et al.*, "Determination of metal impurity density, ΔZ_{eff} and dilution on JET by VUV emission spectroscopy," Plasma Phys. Controlled Fusion **53**, 035009 (2011).
[10]K. D. Lawson, I. H. Coffey, F. Rimini, I. Ksiazek, and JET Contributors, Plasma Phys. Controlled Fusion **63**, 105001 (2021).
[11]N. Krawczyk, A. Czarnecka, I. Ivanova-Stanik, R. Zagorski, C. Challis, D. Frigione, C. Giroud, J. Graves, M. J. Mantsinen, S. Silburn *et al.*, "Application of the VUV and the soft x-ray systems on JET for the study of intrinsic impurity behaviour in neon seeded hybrid discharges," Rev. Sci. Instrum. **89**, 10D131 (2018).
[12]A. Czarnecka, N. Krawczyk, P. Jacquet, E. Lerche, V. Bobkov, C. Challis, D. Frigione, J. Graves, K. D. Lawson, M. J. Mantsinen *et al.*, "Analysis of metallic impurity content by means of VUV and SXR diagnostics in hybrid discharges with hot-spots on the JET-ITER-like wall poloidal limiter," Plasma Phys. Controlled Fusion **61**, 085004 (2019).

[13]T. Pütterich, R. Dux, R. Neu, M. Bernert, M. N. A. Beurskens, V. Bobkov, S. Brezinsek, C. Challis, J. W. Coenen, I. Coffey *et al.*, "Observations on the W-transport in the core plasma of JET and ASDEX Upgrade," Plasma Phys. Controlled Fusion **55**, 124036 (2013).
[14]P. Carvalho, private communication (2023).
[15]E. R. Solano, G. Birkenmeier, E. Delabie, C. Silva, J. C. Hillesheim, A. Boboc, I. S. Carvalho, P. Carvalho, M. Chernyshova, T. Craciunescu *et al.*, "L-H transition threshold studies in helium plasmas at JET," Nucl. Fusion **61**, 124001 (2021).
[16]G. Birkenmeier, E. R. Solano, E. Lerche, D. Taylor, D. Gallart, M. J. Mantsinen, E. Delabie, I. S. Carvalho, P. Carvalho, E. Pawelec *et al.*, "The power threshold of H-mode access in mixed hydrogen-tritium plasmas at JET," Nucl. Fusion **62**, 086005 (2022).
[17]E. Solano, G. Birkenmeier, C. Silva, E. Delabie, J. Hillesheim, A. Baciero, I. Balboa, M. Baruzzo, A. Boboc, M. Brix *et al.*, Nucl. Fusion **63**, 112011 (2023).
[18]A. Chomiczewska, W. Gromelski, I. Ivanova-Stanik, E. Kowalska - Strzeciwilk, N. Wendler, P. Jacquet, A. Meigs, J. Mailloux, S. Menmuir, J. Karhunen *et al.*, "ICRH-related impurity source and control across experiments in H, D, T plasmas at JET-ILW," in IAEA Fusion Energy Conference, 2023.
[19]E. Lerche, "Development of a hybrid plasma scenario for D-T experiments in JET-ILW," in 6th Asia Pacific Conference on Plasma Physics (AAPPS-DPP2022), 2022.